Analytical and experimental bearing capacities of system scaffolds[*]

Jui-lin PENG[†1], Tsong YEN[2], Ching-chi KUO[3], Siu-lai CHAN[4]

(*1Department of Construction Engineering, National Yunlin University of Science and Technology, Taiwan 64002, China*)

(*2Department of Civil Engineering, Chaoyang University of Technology, Taiwan 41349, China*)

(*3Department of Civil Engineering, National Chung-Hsing University, Taiwan 402, China*)

(*4Department of Civil and Structure Engineering, Hong Kong Polytechnic University, Hong Kong, China*)

[†]E-mail: peng.jl@msa.hinet.net

Abstract: We investigated the structural behavior and bearing capacity of system scaffolds. The research showed that the critical load of a system scaffold structure without diagonal braces is similar to that of a door-shaped steel scaffold structure. Joint stiffness between vertical props in system scaffolds can be defined based on a comparison between analytical and experimental results. When the number of scaffold stories increases, the critical loads of system scaffolds decrease. Diagonal braces markedly enhance the critical load of system scaffolds. The coupling joint position between vertical props should be kept away from story-to-story joints to prevent a reduction in critical loads. The critical load of a system scaffold decreases as the quantity of extended vertical props at the bottom of the structure increases. A large Christmas tree set up by system scaffolds under various loads was used as an example for analysis and to check the design of system scaffolds.

Key words: Bearing capacity, Critical Load, System scaffold
doi:10.1631/jzus.A0820010   **Document code:** A   **CLC number:** TU3; TU5

INTRODUCTION

With upgrades to construction methods and automation of some construction processes, modular falsework is always used in the construction field. Traditional frame-type scaffolds have commonly been used as temporary structures. However, frame-type scaffolds use cross-braces to connect each modular scaffold unit in a scaffolding system. This set-up causes frame-type scaffold systems to have two axes, a strong axis and a weak axis. To avoid the weak axis in scaffold systems, a new modular support structure, system scaffold, has been introduced into the construction field.

In comparison with conventional frame-type scaffolds, the system scaffold has the following superior features: (1) no distinction between the strong axis and weak axis; (2) freely-adjustable heights of the jack base; (3) no need to use other shores in the headroom between the scaffold and the formwork; and (4) fast and easy installation based on environmental conditions in construction sites.

The design strength data of the system scaffolds are almost nominal values that do not represent actual material conditions in construction sites. In addition, the system scaffolds produced in Taiwan are copies of system scaffolds from other countries. These copied scaffolds cannot provide appropriate design data. As designers lack verified design parameters for adequate bearing capacity, they may generate incorrect data that would cause the collapse of scaffold structures. Fig.1 shows a collapsed system scaffold in Taiwan.

Most research has focused on strength and failure models of modular frame-type scaffolds. Godley and Beale (1997; 2001) investigated the load-carrying

capacities and failure behaviors of reduced scaffolding models. Yu (2004) examined column curves based on experimental tests of frame-type scaffolds. Huang *et al*.(2000) tested experimentally the bearing capacity of door-type scaffolds and conducted eigenvalue analyses using ANSYS. Peng (2002; 2004) and Peng *et al*.(1996a; 1996b; 1997a; 1997b; 1998; 2001) investigated the bearing capacities and failure models of various falsework including one-layer shoring systems, double-layer shoring systems, and frame-type scaffold systems. Furthermore, Peng *et al*.(1996c; 2003; 2007) examined the effects of fresh concrete load on falsework.

Fig.1 Collapse of system scaffolds at construction sites in Taiwan

Weesner and Jones (2001) explored the experimental load-carrying capacities of system scaffolds. However, their study focused on system scaffolds used when finishing a building facade, and the effect of lateral wind load applied to the scaffolds. Workers typically do not work under high wind conditions. Such a loading situation is considerably different from that experienced during construction.

Many studies of frame-type scaffolds have been conducted; however, the failure behaviors of frame-type scaffolds differ from those of system scaffolds. This study will help to overcome the lack of analysis and design data for system scaffolds. By identifying failure behaviors and bearing capacities of system scaffolds, it will contribute to the safety of these temporary structures in construction sites.

INSTALLATION, MATERIAL PROPERTIES AND ANALYSIS

Installation

A system scaffold comprises three steel tubes, i.e., a vertical prop, a horizontal bar and a diagonal brace (Fig.2). Fig.2 shows a joint connected with a specific coupling between two vertical props. Fig.3a shows this coupling style for joint connection.

A circular plate with pre-drilled holes is welded onto the vertical prop. Horizontal bars and diagonal braces are then inserted into these holes. Fig.3b shows four horizontal bars coupled into the holes. Fig.3c shows a diagonal brace inserted into a hole.
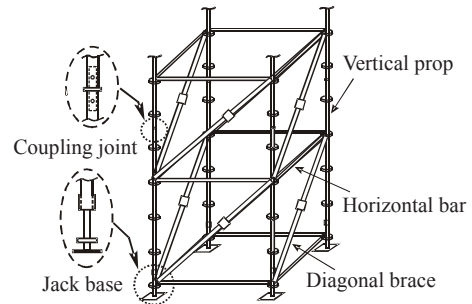

Fig.2 Set-up and accessories of system scaffold

(a)

(b)

(c)

Fig.3 Coupling style (a) between vertical props, (b) for horizontal bars of a system scaffold and (c) for horizontal bars and a diagonal brace of a system scaffold

In a system scaffold, a jack base 35 cm high is set up on the ground. This jack base connects horizontal bars inserted into the holes on the welded circular plate (Fig.4). The system scaffold is extended to become a large-scale structural system via vertical props, horizontal bars, diagonal braces and coupling joints.

Fig.4 Jack base of a system scaffold

Material properties

The system scaffold material properties are a cross-sectional area of steel tube A, moment of area I and elastic modulus E. The cross-sectional area A for the vertical prop is 3.982 cm^2, the moment of area I_y ($=I_z$) is 10.747 cm^4, and the elastic modulus E is 20012.4 kN/cm^2 (2040 t/cm^2; 1 kN/cm^2=1 t/cm^2× 9.81 N/kg). For the horizontal bar and diagonal brace, both cross-sectional areas A are 3.794 cm^2, the moment of area I_y ($=I_z$) is 10.668 cm^4, and the elastic modulus E is 20012.4 kN/cm^2 (2040 t/cm^2).

Numerical analysis

In this study, the bearing capacities of system scaffolds were calculated based on 3D structural analysis. A second-order elastic semi-rigid-joint analysis, i.e., geometric nonlinear/material linear/ semi-rigid-joint analysis, was used. To simulate initial imperfections within the system scaffold, the notional lateral forces applied on various system scaffolds were 0.1%~0.5% of the total vertical load. This study used the computer program GMNAF (Geometry and Material Nonlinear Analysis of Frame) developed by Chan (1988), Chan and Zhou (1994), and Chan and Cho (2005).

In the GMNAF computer program, a fifth-order polynomial y can be found by calculation from six boundaries. The displacement y will be converted to the cubic Hermite function if the axial force P is zero. The discrepancy between the cubic element and the present fifth-order element increases when the axial force P is large.

TEST OF 2-STORY SYSTEM SCAFFOLDS

The experimental test for the 2-story system scaffold generated necessary reference data for analysis. Fig.5 shows the set-up of the 2-story system scaffold structure without diagonal braces. The diagonal braces were removed from the system scaffold structure to obtain the lower bound of the critical load. The tested critical load can be adopted as a reference for designing the bearing capacity of a 2-story system scaffold structure in construction sites. In addition, exclusion of diagonal braces removes the joint stiffness of diagonal braces from the system scaffold, which facilitates verification of the joint stiffness between vertical props in the analysis.

Fig.5 Installation of a 2-story system scaffold without diagonal braces before loading

Fig.6 shows the set-up and dimensions of the 2-story system scaffold. Except for the diagonal braces, the set-up was based on real installations in construction sites in Taiwan. In accordance with the headroom of buildings during construction, an extra shoring length must be considered since the headroom is not just a multiple of system height (180 cm). In this study, four additional vertical props, each 60 cm high, were added to the 2-story system scaffold. Fig.6 shows the detailed adjustment dimensions.

Fig.7 shows the tested deformation shape of the system scaffold after loading. The failure behavior of the system differs from that of conventional frame-type scaffolds. The tested critical load of the 2-story system scaffold without diagonal braces was 131.9 kN (13.442 t), which is not superior to that of a simple 2-story door-type frame scaffold with jack bases.
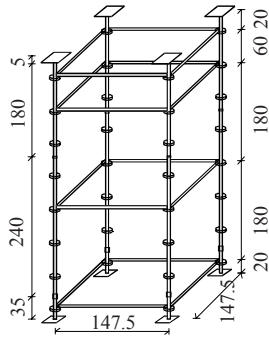
Fig.6 Test set-up and dimensions of a 2-story system scaffold without diagonal braces (unit: cm)

Fig.7 Deformation shape of a 2-story system scaffold without diagonal braces

ANALYTICAL RESULTS AND COMPARISONS

Effect of boundary conditions

The boundary conditions (BCs) and joint stiffness of the system scaffold were analyzed first. BCs based on the system scaffold set-up were of two types: fixed end and hinged end. Changing the joint stiffness of the system scaffold altered the critical load. In addition, the fixed end and hinged end can be regarded as the upper bound and lower bound of bearing capacities, respectively, for the system scaffold. In reality, the strength of a system scaffold in construction sites should be between the upper and lower bounds. To simplify analyses, the joint stiffness of vertical props and pedestals was assumed to be identical since these two positions have the same coupling. The top and bottom boundary conditions of the system scaffold were also identical because their base-plates were almost the same. The joint stiffness of horizontal bars was considered to be that of a rigid joint.

Fig.8 shows the relationship between joint stiffness and critical load for the 2-story system scaffold without diagonal braces based on different boundary conditions. The horizontal axis in Fig.8 represents the joint stiffness of vertical props, and the vertical axis is the critical load of the structure. The trend of the curves for the two boundary conditions is approximately linearly ascending as joint stiffness increases. The small difference between the two curves and their parallel tendency indicate that the effects of different boundary conditions on the system scaffold are minimal (Fig.8). The major reason for these minimal effects is the good lateral supporting effect from the structure base and top with four horizontal bars comprising a rectangle adjacent to the boundary ends of the structure.
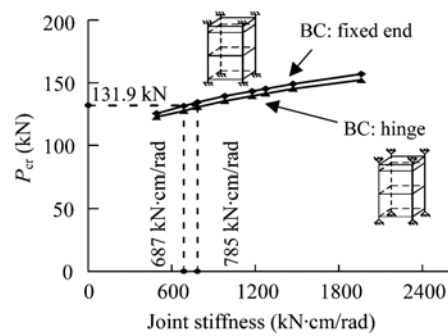

Fig.8 Critical loads P_{cr} vs joint stiffnesses of a 2-story system scaffold without diagonal braces based on different boundary conditions

Fig.9 shows the deformation shape of the system scaffold after loading. Since similar analytical results were obtained for various joint stiffnesses, Fig.9 shows the analytical result for a joint stiffness of 785 kN·cm/rad (80 t·cm/rad) for the hinged boundary case. Fig.10 shows the curve of load vs displacement (P-Δ curve). When the curve approaches a fixed value, the value of this converged asymptote is the critical load of the system scaffold.

Prediction of joint stiffness

The joints in the system scaffold were of three types: (1) joints for vertical props (Fig.3a); (2) joints for horizontal bars (Fig.3b); and (3) joints for diagonal braces (Fig.3c). The first joint type was connected by a specific curl-pin coupling two vertical props (Fig.3a). The second joint type was a specific connection on a thick plate welded onto a vertical prop. A pin was inserted into the hole of the thick plate to

connect a horizontal bar (Fig.3b). This solid coupling connection, in addition to the welded part, makes joint stiffness relatively high. The third joint type (Fig.3c) had a hinged-joint mechanism linking it to the second joint type (Fig.3a).
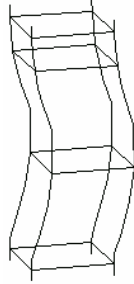

Fig.9 Deformation shape of a 2-story system scaffold without diagonal braces after loading (BC: hinge; joint stiffness: 785 kN·cm/rad)
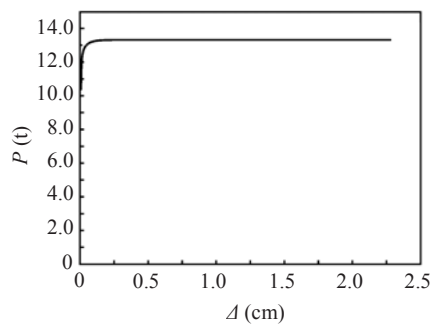

Fig.10 Load-deflection curve of a 2-story system scaffold without diagonal braces (1 kN=1 t×9.81 N/kg)

For analysis, the joint assumption must first be simplified. Three joint stiffnesses were considered. For the joint stiffness where vertical props connect, a semi-rigid joint was used to simulate the real set-up. The joint stiffness of the horizontal bar was simulated as that of a rigid joint since its special coupling style significantly increases stiffness. Joint stiffness of the diagonal brace was assumed to be that of a hinged joint because of its special hinged mechanism (Fig.3c).

Fig.11 presents the relationship between applied moment and rotation angle for a semi-rigid joint. The stiffness curve of the semi-rigid joint is nonlinear, except for the small rotation angle at the initial stage. Based on scaffolding research (Peng *et al*., 1997a; 1998), deformation of the scaffold structure is small before a scaffold structure fails. Thus, stiffness k_s in the linear segment of the curve (Fig.11) is the joint stiffness of vertical props.
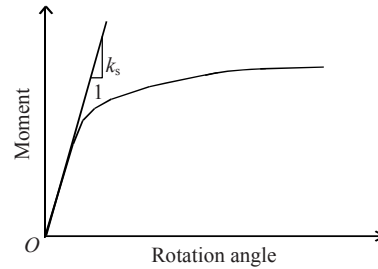

Fig.11 Moment-rotation angle curve of a semi-rigid joint

The joint stiffness of vertical props can be derived by comparison of test results and analysis of critical loads of the system scaffold. The critical load of the test result for the 2-story system scaffold was 131.9 kN (13.4 t). A horizontal line drawn from this point that crosses the curve (Fig.8), gives the corresponding joint stiffness, which is 687 kN·cm/rad (70 t·cm/rad) for the fixed end and 785 kN·cm/rad (80 t·cm/rad) for the hinged-end boundary condition. Since jack bases are seldom used in real construction sites, the boundary conditions at ends of this system scaffold are considered hinged-ends. Thus, the joint stiffness of the vertical props was 785 kN·cm/rad in subsequent analyses.
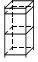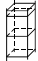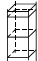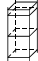
Effects of different base heights

The effect of different base heights on the ground on the critical load of the system scaffold was investigated. The analtical model was based primarily on the system scaffold set-up, and vertical props were added to the base story to simulate height differences. The heights of the extended vertical props added at the bottom were 60 cm and 120 cm. The top and bottom boundary conditions were hinges and the joint stiffness was 785 kN·cm/rad (80 t·cm/rad) in the analysis.

Table 1 lists the analytical results for critical loads of the system scaffolds with different base heights. The different base heights on the ground varied depending on the positions of vertical props located at the bottom. This study investigated six different heights. Table 1 shows the set-up for all different base heights. Case A was a system scaffold without vertical props. Case B had one extended vertical prop at the bottom. Case C_1 had two extended vertical props set-up in a diagonal configuration. Case C_2 had two extended vertical props set-up on the same side. Case D had three extended vertical props set-up

on the bottom. Case E had four extended vertical props set-up at the bottom.

Table 1 Critical loads of system scaffolds with different base heights

Height case		Critical load (t)	
		60 cm	120 cm
A		130.5 (13.3)	130.5 (13.1)
B		128.5 (13.1)	127.5 (13.0)
C_1		127.5 (13.0)	126.5 (12.9)
C_2		115.8 (11.8)	96.1 (9.8)
D		69.7 (7.1)	60.8 (6.2)
E		65.7 (6.7)	55.9 (5.7)

Date in parentheses mean critical loads in t, 1 kN=1 t×9.81 N/kg; Case A is the basic set-up of 2-story system scaffold; Cases B~E simulate uneven bases of system scaffolds with 60 cm and 120 cm

Fig.12 shows the relationship between critical loads of the system scaffolds and different heights of extended vertical props at the bottom. As the quantity of extended vertical props increases, the critical load of the system scaffold decreases. The critical load for Case C_1 with extended vertical props forming a diagonal line was higher than that of Case C_2 with single-side vertical props (Fig.12 and Table 1). The critical loads of Case C_1 and Case B were similar. By adding three and four extended vertical props to the bottom, as in Cases D and E, the critical loads of the system scaffolds decreased by 50%. Thus, these two configurations should be avoided.
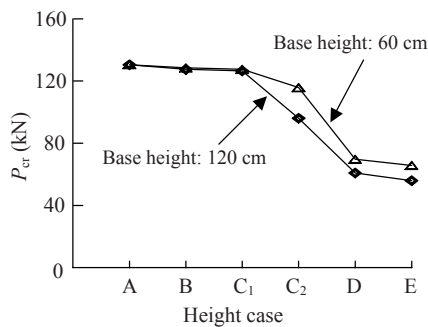

Fig.12 Comparison of critical loads of system scaffolds with different base heights

Effects of scaffold height

The effect of the number of stories on the system critical load was investigated. The analysis of critical load was based on a 2-story system scaffold structure with its height extended to a 10-story structure. To simplify analyses, an integration of boundary conditions and joint stiffness values that coincided with the test value of 131.9 kN, was used in the analyses. The analytical models were as follows: (1) The top and bottom BCs were both the fixed ends and the joint stiffness was 687 kN·cm/rad (70 t·cm/rad); and (2) The top and bottom BCs were both the hinged ends and the joint stiffness was 785 kN·cm/rad (80 t·cm/rad).

Fig.13 shows the relationship between the critical load and story number. The similarity between critical loads under the two analytical models indicates that both models can be used as basic models for theoretical analyses. The critical load of the system scaffolds decreased as the number of stories increased; a fixed value (about 75 kN) is seen during a convergence of the curves in Fig.13. This characteristic is extremely similar to the column curve in stability analysis.
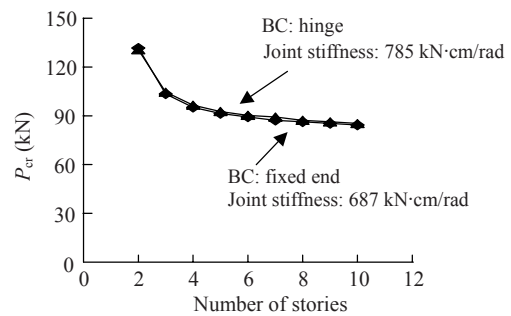

Fig.13 Critical loads P_{cr} of system scaffolds with various numbers of stories based on different joint stiffnesses and boundary conditions

Fig.14 shows the deformation shape of an 8-story system after loading. Because each of the top two rectangular frames was encircled by four horizontal bars to increase bending moment resistance, the boundary conditions of the entire structure resemble the instance with top fixed ends and bottom hinged ends. As the structure had no diagonal braces, no bracing effect exists.

Fig.14 Deformation shape of an 8-story system scaffold after loading (BC: hinge; joint stiffness: 785 kN·cm/rad; joint position: Case A in Table 1)

Effects of diagonal brace installations

Diagonal braces are necessary when constructing system scaffolds in construction sites. The primary objective in this section was to determine the effect of various diagonal brace positions on the critical load of a system scaffold. The analytical model was based on a 2-story system scaffold with four diagonal braces added to each story. The scaffold structures considered in the analysis ranged from 2 to 10 stories. Hinges were considered at the top and bottom boundary conditions, and the joint stiffness was 785 kN·cm/rad.

Fig.15 illustrates three configurations for the system scaffolds with added diagonal braces. Case A shows the set-up of parallel face-to-face diagonal braces and parallel story-to-story coplanar diagonal braces. Case B shows the set-up of the reversed parallel story-to-story diagonal braces and parallel story-to-story coplanar diagonal braces. Case C shows the set-up of reversed parallel face-to-face diagonal braces and intersection of story-to-story coplanar diagonal braces. Case A is a common set-up for diagonal braces in construction sites in Taiwan.
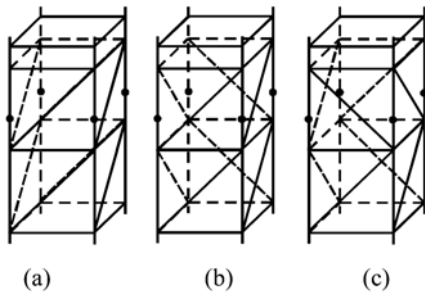

Fig.15 Different bracing installations of a 2-story system scaffold. (a) Case A; (b) Case B; (c) Case C

Fig.16 shows a comparison of critical loads of the system scaffolds with various diagonal braces. The critical loads were markedly increased when diagonal braces were added to the structure. For the set-up of diagonal braces, Case B (Fig.15) had the highest critical load for these three cases, as the set-up of diagonal braces in Case B bears horizontal forces. Thus, we recommend that the set-up in Case B be used in construction sites.
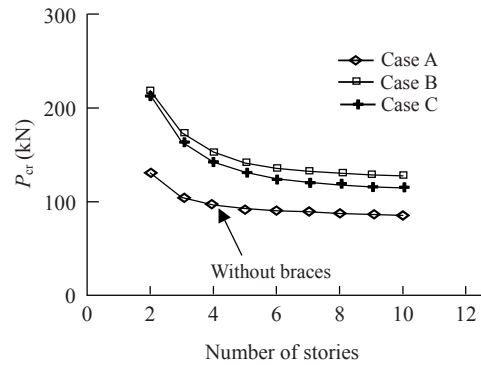

Fig.16 Critical loads P_{cr} vs number of stories of system scaffolds with different installed diagonal braces in Fig.15

Fig.17 shows a failure deformation of an 8-story system scaffold with the set-up in Case B of Fig.15. This failure situation differs from that in Fig.14 owing to the bracing effects of diagonal braces. No obvious deformation occurred at the joints of central horizontal bars but arresting deformation occurred at the joints of vertical props.

Fig.17 Deformation shape of an 8-story system scaffold (Case B in Fig.15) after loading (BC: hinge; joint stiffness: 785 kN·cm/rad)

Effect of joint positions

The critical loads of the system scaffolds with different joint positions were investigated. Fig.18 is a drawing of different joint positions in the system scaffold. In Case A (Fig.18), the joint positions were

on identical planes 240 cm above the joints on the bottom story; the base height was 35 cm. In Case B_1, two joints at symmetrical diagonal positions were lowered to a position of 180 cm from the joints on the bottom story. In Case B_2, two joints located on the same side of the scaffold were lowered to 180 cm from the joints on the bottom story. In Case C, four joints were on an identical plane 180 cm from the joints on the bottom story.
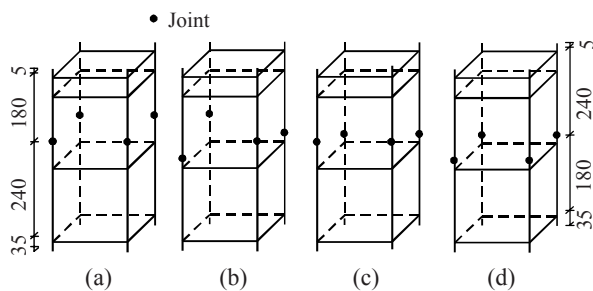

Fig.18 Different joint positions of system scaffolds used in construction sites (unit: cm). (a) Case A; (b) Case B; (c) Case C; (d) Case D

Fig.19 shows the relationship between critical load and various joint positions without diagonal braces based on different numbers of stories in the system scaffolds shown in Fig.18. The critical load of the system scaffold in Case A was superior to those of other cases; notably, Case C was weakest. The configurations of joint positions in Cases B_1 and B_2 were combinations of the configurations in Cases A and C. Thus, the critical loads for Cases B_1 and B_2 were between those for Cases A and C.
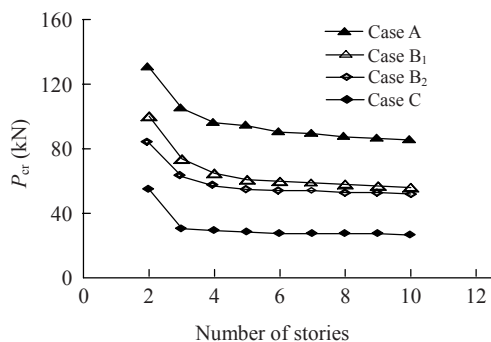

Fig.19 Critical loads vs number of stories of system scaffolds with different joint positions in Fig.18

The fact that joint positions in Case B_1 were symmetrical may have contributed to a better critical load in Case B_1 than in Case B_2. This analytical result was similar to that for different base heights (subsection "Effects of different base heights"). Inefficiency in transmission of horizontal forces and reduced critical load can occur when joints on vertical props are near the story-to-story joints. Since joint positions in Case C were adjacent to story-to-story joints (i.e., joints of horizontal bars), its critical load was low. Thus, for coupling of vertical props in the system scaffold, joint positions should be kept away from story-to-story joints.

Fig.20 shows a failure deformation of an 8-story system scaffold after loading. The joint positions on the vertical props of this scaffold structure are arranged as in Case B_2. The failure point is located on the joints of the vertical props adjacent to story-to-story joints. The failure model of this system scaffold (Fig.20) differs from that shown in Fig.14.

Fig.20 Deformation shape of an 8-story system scaffold (Case B_2 in Fig.18) after loading (BC: hinge; joint stiffness: 785 kN·cm/rad)

Analysis of a real example

On Christmas Day 1997, a giant Christmas tree set up by a 14-story system scaffold was erected in the Encore Garden in Taichung, Taiwan (Fig.21). The height of each story of the scaffold was 180 cm, and

Fig.21 Arrangement of a Christmas tree after construction and decoration in Encore Garden

the height of the top story was 60 cm. The vertical load was from artificial leaves, ornaments and pre-stressed steel cords on the Christmas tree. The horizontal load was from lateral wind forces. For this system scaffold, a joint stiffness of 785 kN·cm/rad was selected for the second-order/elastic/semi-rigid joint analysis.

Vertically uniform load

When a vertically uniform load was applied to the Christmas tree structure, the critical load of the system scaffold was 3982 kN (405.9 t). Fig.22 presents the failure shape of the system scaffold of the Christmas tree under vertically uniform loading.

(a)   (b)

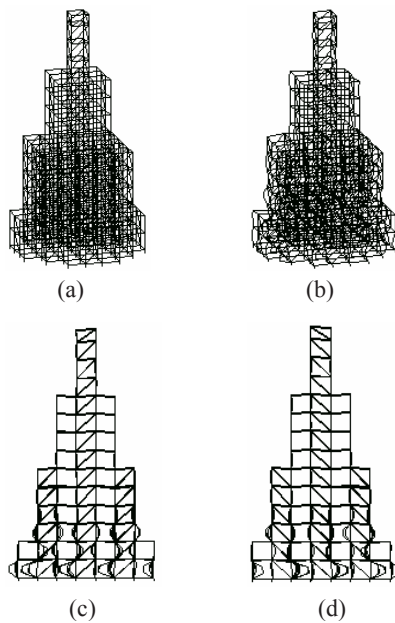(c)   (d)

Fig.22 Deformation shape of a Christmas tree installed by system scaffolds under vertically uniform load. (a) Before loading; (b) After loading; (c) Front-view after loading; (d) Side-view after loading

Lateral wind force

Fig.23 shows the following four types of lateral wind loads: (a) lateral load concentrated at the top; (b) inverse triangle-shaped lateral load; (c) uniform lateral load; and (d) lateral load based on the Code of Construction Technology (1997) for Taiwan. The concentrated load simulated the lower bound of bearing capacity and the uniform load simulated the upper bound of bearing capacity. The inverse triangle-shaped lateral load was located between the upper and lower bounds. The fourth load type was used for analyses using specifications for wind load in the

Code of Construction Technology (1997) for Taiwan. Analytical results are as follows:

(1) The concentrated load at the top resulted in a 43.2 kN (4.4 t) failure load on the Christmas tree structure. Fig.24 presents the *P-Δ* curve.

(2) The inverse triangle-shaped lateral load generated a 239.4 kN (24.4 t) failure load on the Christmas tree structure, which is roughly 5.5 times higher than the concentrated lateral load.

(3) The uniform lateral load caused a 596.4 kN (60.8 t) failure load on the Christmas tree structure, which is approximately 14 times higher than that for the concentrated lateral load.

(4) According to specifications for wind loads in the Code of Construction Technology (1997) for Taiwan, this Christmas tree was positioned in a 150-class wind area. Wind pressure in this area is 110 kg/m² at heights <9 m, 150 kg/m² for heights of 9~15 m, and 190 kg/m² for heights of 15~30 m (Fig.23d). Based on this lateral load, the failure load for the Christmas tree structure was 262.9 kN (26.8 t), roughly 6 times higher than the concentrated lateral
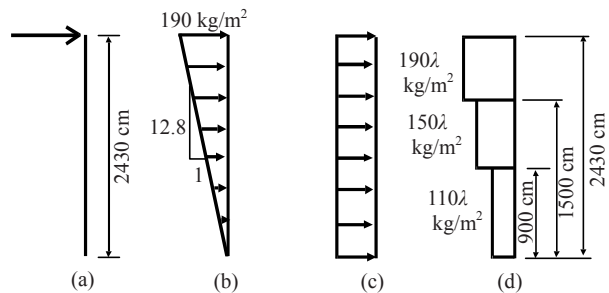

(a)   (b)   (c)   (d)

Fig.23   Different lateral wind forces applied to a Christmas tree. *λ* is the load factor, used in the nonlinear analysis. (a) Concentrated load; (b) Triangle load; (c) Uniform load; (d) Code load
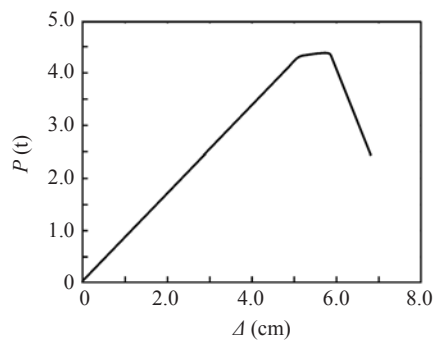

Fig.24 *P-Δ* curve of a Christmas tree installed by system scaffolds caused by a concentrated lateral load applied at the top (1 kN=1 t×9.81 N/kg)

load. Additionally, this failure load is between the inverse triangle-shaped lateral load and the uniform lateral load. After the load was applied to the structure, deformation-inducing failure was located on the top extension (Fig.25).

Based on these analyses, bearing capacity under vertically uniform loading was extremely high, and actual vertical design loads should not destroy the scaffold structure. When lateral wind loads vary, failure loads for the tree structure differ. As the lateral load acting on the structure height increases, the failure load of the entire structure decreases. This analytical result can be used as a reference when designing a Christmas tree installed by system scaffolds.
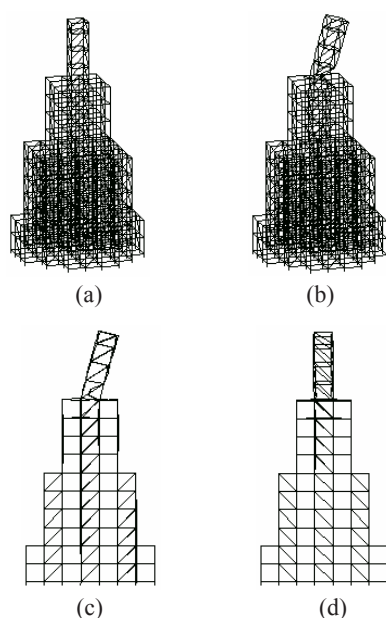

Fig.25 Deformation shape of a Christmas tree installed by system scaffolds caused by wind load based on specifications. (a) Before loading; (b) After loading; (c) Front-view after loading; (d) Side-view after loading

CONCLUSION

Based on analyses and discussions, a number of important conclusions are obtained.

(1) The critical load of a system scaffold without diagonal braces is similar to that of a door-shaped steel tube scaffold with the same number of stories and jack bases.

(2) The four horizontal bars adjacent to structure boundaries may weaken the effect of hinged and fixed

boundary conditions on the critical load of system scaffolds.

(3) Joint stiffness between vertical props in system scaffolds was 785 kN·cm/rad (80 t·cm/rad) in this study.

(4) As the quantity of extended vertical props at the structure bottom increases, the critical load of the system scaffold decreases gradually.

(5) As the number of stories of a system scaffold increases, the critical load of the structure decreases.

(6) Diagonal braces substantially enhance the critical load of a system scaffold. Thus, we recommend that Case B—the set-up of reversed parallel story-to-story diagonal braces and parallel story-to-story coplanar diagonal braces—should be installed to markedly increase the bearing capacity of a system scaffold.

(7) The coupling joint positions between vertical props should be kept away from story-to-story joints (i.e., horizontal bar joints) to prevent the weakening of critical loads of system scaffolds.

(8) According to wind specifications in the Code of Construction Technology for Taiwan, the failure load of the large-sized Christmas tree installed using system scaffolds in the Encore Garden of Taichung, Taiwan, was 262.9 kN.

References

Chan, S.L., 1988. Geometric and material nonlinear analysis of beam-columns and frames using the minimum residual displacement method. *International Journal for Numerical Methods in Engineering*, **26**(12):2657-2669. [doi:10.1002/nme.1620261206]

Chan, S.L., Cho, S.H., 2005. Second-order *P-Δ-δ* analysis and design of angle trusses allowing for imperfections and semi-rigid connections. *International Journal of Advanced Steel Construction*, **1**(1):157-172.

Chan, S.L., Zhou, Z.H.A., 1994. Pointwise equilibrium polynomial (PEP) element for nonlinear analysis of frame. *Journal of Structural Engineering ASCE*, **120**(6):1703-1717. [doi:10.1061/(ASCE)0733-9445(1994)120:6(1703)]

Code of Construction Technology, 1997. Ministry of the Interior, Construction and Planning Agency, Taiwan (in Chinese).

Godley, M.H.R., Beale, R.G., 1997. Sway stiffness of scaffold structures. *The Structural Engineer*, **75**(1):4-12.

Godley, M.H.R., Beale, R.G., 2001. Analysis of large proprietary access scaffold structures. *Proceedings of the Institution of Civil Engineers Structures & Buildings*, **146**(1):31-39.

Huang, Y.L., Chen, H.J., Rosowsky, D.V., Kao, Y.G., 2000. Load-carrying capacities and failure modes of scaffold-shoring systems, part I: modeling and experiments. *Structural Engineering and Mechanics*, **10**(1):53-66.

Peng, J.L., 2002. Stability analyses and design recommendations for practical shoring systems during construction. *Journal of Construction Engineering and Management ASCE*, **128**(6):536-544. [doi:10.1061/(ASCE)0733-9364 (2002)128:6(536)]

Peng, J.L., 2004. Structural modeling and design considerations for double-layer shoring systems. *Journal of Construction Engineering and Management ASCE*, **130**(3): 368-377.   [doi:10.1061/(ASCE)0733-9364(2004)130:3 (368)]

Peng, J.L., Rosowsky, D.V., Pan, A.D., Chen, W.F., Chan, S.L., Yen, T., 1996a. Analysis of concrete placement load effects using influence surfaces. *Structural Journal ACI*, **93**(2):180-186.

Peng, J.L., Pan, A.D., Rosowsky, D.V., Chen, W.F., Yen, T., Chan, S.L., 1996b. High clearance scaffold systems during construction-I. structural modelling and modes of failure.   *Engineering   Structures*, **18**(3):247-257. [doi:10.1016/0141-0296(95)00144-1]

Peng, J.L., Rosowsky, D.V., Pan, A.D., Chen, W.F., Chan, S.L., Yen, T., 1996c. High clearance scaffold systems during construction-II. structural analysis and development of design guidelines. *Engineering Structures*, **18**(3):258-267.

[doi:10.1016/0141-0296(95)00145-X]

Peng, J.L., Yen, T., Lin, I., Wu, K.L., Chen, W.F., 1997a. Performance of scaffold frame shoring under pattern loads and load paths. *Journal of Construction Engineering   and   Management   ASCE*, **123**(2):138-145. [doi:10.1061/(ASCE)0733-9364(1997)123:2(138)]

Peng, J.L., Pan, A.D.E., Chen, W.F., Yen, T., Chan, S.L., 1997b. Structural modeling and analysis of modular falsework systems. *Journal of Structural Engineering ASCE*, **123**(9):1245-1251. [doi:10.1061/(ASCE)0733-9445(1997) 123:9(1245)]

Peng, J.L., Pan, A.D.E., Chan, S.L., 1998. Simplified models for analysis and design of modular falsework. *Journal of Constructional   Steel   Research*,   **48**(2/3):189-209. [doi:10.1016/S0143-974X(98)00198-9]

Peng, J.L., Pan, A.D.E., Chen, W.F., 2001. Approximate analysis method for modular tubular falsework. *Journal of Structural Engineering ASCE*, **127**(3):256-263. [doi:10.1061/(ASCE)0733-9445(2001)127:3(256)]

Peng, J.L., Wu, C.L., Chan, S.L., 2003. Sequential pattern load modeling and warning—system plan in modular falsework.   *Structural   Engineering   and   Mechanics*, **16**(4):441-468.

Peng, J.L., Chan, S.L., Wu, C.L., 2007. Effects of geometrical shape and incremental loads on scaffold systems. *Journal of Constructional Steel Research*, **63**(4):448-459. [doi:10.1016/j.jcsr.2006.07.006]

Weesner, L.B., Jones, H.L., 2001. Experimental and analytical capacity of frame scaffolding. *Engineering Structures*, **23**(6):592-599. [doi:10.1016/S0141-0296(00)00087-0]

Yu, W.K., 2004. An investigation into structural behaviour of modular steel scaffolds. *Steel and Composite Structures*, **4**(3):211-226.